The inherent link between ore formation and geometallurgy as documented by complex tin mineralization at the Hämmerlein deposit (Erzgebirge, Germany)

Kern, M.; Kästner, J.; Tolosana-Delgado, R.; Jeske, T.; Gutzmer, J.;

Originally published:

August 2018

Mineralium Deposita 54(2019)5, 683-698

DOI: https://doi.org/10.1007/s00126-018-0832-2

The inherent link between ore formation and geometallurgy as documented by complex tin mineralization at the Hämmerlein deposit (Erzgebirge, Germany)

Marius Kern [1] · Julian Kästner [1,2] · Raimon Tolosana-Delgado [1] · Tilman Jeske [2] · Jens Gutzmer [1,2]

Abstract
A comprehensive quantitative mineralogical study on the Hämmerlein tin deposit in the Erzgebirge, Germany, not only yields insights into the genesis of Sn mineralization but also provides also important clues for beneficiation. The lithological units of the skarn and greisen deposit show significant differences in modal mineralogy and Sn deportment. These systematic differences are attributed to several stages of ore formation. Of greatest significance is a paragenetically late cassiterite-chlorite-fluorite-sulfide assemblage. This assemblage replaces pre-existing skarn lithologies and also forms stockwork mineralization in greisen-type ores developed at the expense of mica schist that surrounds the skarn. The co-genetic formation of the cassiterite-chlorite-fluorite-sulfide assemblage is captured by the mineral association parameter—a parameter that can be easily quantified from data acquired during automated mineralogy studies. To document the preferred mineral association, a ratio is introduced that illustrates how closely cassiterite—the only Sn mineral of economic relevance—is associated with chlorite, fluorite, and sulfides. This so-called MAMA ratio illustrates the strongly preferred association between cassiterite and chlorite. The results also illustrate that the abundance of rock-forming chlorite may be used as a proxy for the abundance of the much less common cassiterite. This proxy is well-suited to sort ore from poorly mineralized/unmineralized rock fragments early during the beneficiation process. Such separation may well be achieved by using a short wave infrared detector that is already deployed in commercially available sorting equipment. The case study illustrates the inherent link between the processes responsible for ore genesis, the definition of geometallurgical domains, and the selection of suitable beneficiation strategies.

Introduction

For centuries the Erzgebirge, straddling the border between Germany and the Czech Republic, has been a prime source of tin. Most Sn production has been from large greisen deposits, such as Altenberg (Weinhold 2002), Ehrenfriedersdorf (Hösel 1994), and Geyer (Hösel 1995). Although several Sn skarn deposits are well-known across the Erzgebirge—with known resources on the order of ~ 500,000 t of contained Sn (Bock 2009)—they have never been mined on an industrial scale and there is only very limited information available for these skarn deposits in the published literature (e.g., Schuppan and Hiller 2012). Thus, there is a distinct lack of understanding of the geology, mineralogy, and beneficiation characteristics. Yet, one of these skarn deposits, the Hämmerlein deposit, is widely regarded as among the most promising undeveloped Sn skarn deposits globally (ITRI 2016).

Since 2015, a nationally funded consortium has been conducting beneficiation test work on cassiterite-bearing ore from the Hämmerlein deposit. Five bulk samples were studied to constrain the Sn deportment of the different skarn lithounits. The complex mineralogy required modification of the conventional approach of automated mineralogy as documented by Kern et al. (2018). Besides cassiterite

✉ Marius Kern
m.kern@hzdr.de

[1] Helmholtz-Zentrum Dresden-Rossendorf, Helmholtz Institute Freiberg for Resource Technology, Chemnitzer Straße 40, 09599 Freiberg, Germany

[2] Institute of Mineralogy, Technische Universität Bergakademie Freiberg, Brennhausgasse 14, 09599 Freiberg, Germany

(SnO_2), there are several other minerals that contribute significantly to the Sn content of bulk ore samples, including stokesite ($CaSnSi_3O_9 \times 2H_2O$) with a median Sn content (MSn) of 34.2 wt%, titanite (MSn = 3.9 wt%), epidote (MSn = 1.3 wt%), and iron oxide minerals (MSn = 0.8 wt%). Lattice-bound Sn in typically Sn-poor rock-forming minerals is known from many other skarn deposits such as Lost River, Alaska (Dobson 1982), Land's End Aureole in Cornwall (van Marcke de Lummen 1986) or Mt. Lindsay, Tasmania (Eadington and Kinealy 1983). Although the amount of Sn and the variety of different Sn-bearing minerals is remarkably high at Hämmerlein, cassiterite remains the only Sn-bearing mineral that is of commercial interest.

This study documents the link between Sn deportment for the different lithological units of the Hämmerlein deposit and ore genesis. Results are based on field geological observations as well as detailed investigations of a large suite of hand specimens. In addition, bulk samples were analyzed with the goal to test the relevance of mineral associations documented at hand specimen scale for the development of a successful mineral beneficiation strategy.

Geological setting

The Hämmerlein deposit in the Western Erzgebirge is an example of a compositionally complex and polymetallic ore deposit that comprises two parts: a Sn-In-Zn skarn and a greisenized shale called *Schiefererz* (Schuppan and Hiller 2012). It is part of a much larger ore-forming system as it is closely associated with the tin-tungsten orebody of Pöhla-Globenstein (Hösel 2003) and the Tellerhäuser deposit with the tin-uranium orebodies of Dreibach and Zweiberg, hosted by metamorphic rocks of the Variscan Jachymov and Thum groups (Schuppan and Hiller 2012) (Fig. 1b). The distance to the underlying 320 Ma Eibenstock-type granite (Romer et al. 2006; Tichomirowa and Leonhardt 2010; Zhang et al. 2017) is between 200 and 500 m (Fig. 1c). Schuppan and Hiller (2012) review the available literature and the exploration history commencing with discovery of the skarn deposits in 1966 until the early 1990s, when interest waned due to the breakdown of the former GDR. Exploration and related research resumed only recently.

The laterally extensive stratabound skarn has a thickness of 2–20 m (Schuppan and Hiller 2012) and comprises four distinct lithounits of consistent geometallurgical, mineralogical and physical characteristics:

- Feldspar-pyroxene-epidote lithounit (FPEL)
- Garnet lithounit (GL)
- Iron oxide lithounit (IOL)
- Amphibole lithounit (AL)

Underground face mapping (Kästner 2016, Fig. 2) illustrates that these lithounits not only often display semi-conformable relations but are also found to be laterally discontinuous. Considering the relative distance to the causative pluton, the protolith to the four lithounits is expected to be a Ca-Mg-rich unit of sedimentary origin (Meinert et al. 2005). The four lithounits are invariably enriched in Sn, which is not only hosted in cassiterite but also in silicates and iron oxides (Kern et al. 2018; Schuppan and Hiller 2012). Locally, the skarn carries significant mineralization of sphalerite that may be enriched in In (Bauer et al. 2017); both Zn and In are considered as likely by-products during eventual mining of the Hämmerlein deposit (Treliver Minerals Limited 2015). The skarn is surrounded by mica schist (MS) and granitic gneiss (GS), which are both extensively altered (Miehlbradt 2017; Winkler 2017). Locally, the mica schist is crosscut by 1–2-cm-thick veinlets that contain abundant cassiterite where in direct contact to the skarn. This so-called *Schiefererz*, which literally translated means *schist ore*, is considered part of the resource (Schuppan and Hiller 2012; Miehlbradt 2017).

Sn-In-Zn mineralization is clearly postdated by crosscutting pitchblende-quartz-fluorite mineralization. Although this vein-style mineralization is particularly prominent in the nearby Tellerhäuser deposit, it is also observed at the Hämmerlein deposit (Schuppan and Hiller 2012).

Materials and methods

Accessibility of the Hämmerlein deposit is excellent. Access to extensive underground mine workings—developed for the exploitation of uranium and bulk trial mining for the skarn ores during GDR times—is provided by the visitors mine *Besucherbergwerk Zinnkammern Pöhla*. The results presented in this study are based on the investigation of a comprehensive suite of hand specimens as well as bulk samples from skarn and Schiefererz from different sites within the Hämmerlein deposit.

Materials

The samples originate from five sampling locations on the + 590 m level (Fig. 3). Localities Strecke 2-4 (S2-4), Strecke 2-6b (S2-6b), Strecke 4 (S4), and Querschlag 2 (Q2) sample the skarn orebody. The Hauptstollen (HS) locality was used to sample mica schist with cassiterite mineralization (Schiefererz).

Sample locations were mapped in detail by Kästner (2016) and Miehlbradt (2017). A comprehensive suite of hand specimens (10–20 cm in diameter) from the host rocks and from the four skarn lithounits was collected. Hand specimens that showed a representative distribution of characteristic minerals were chosen for the preparation of polished thin sections. The remainder of the samples was crushed by hammer (< 3 cm

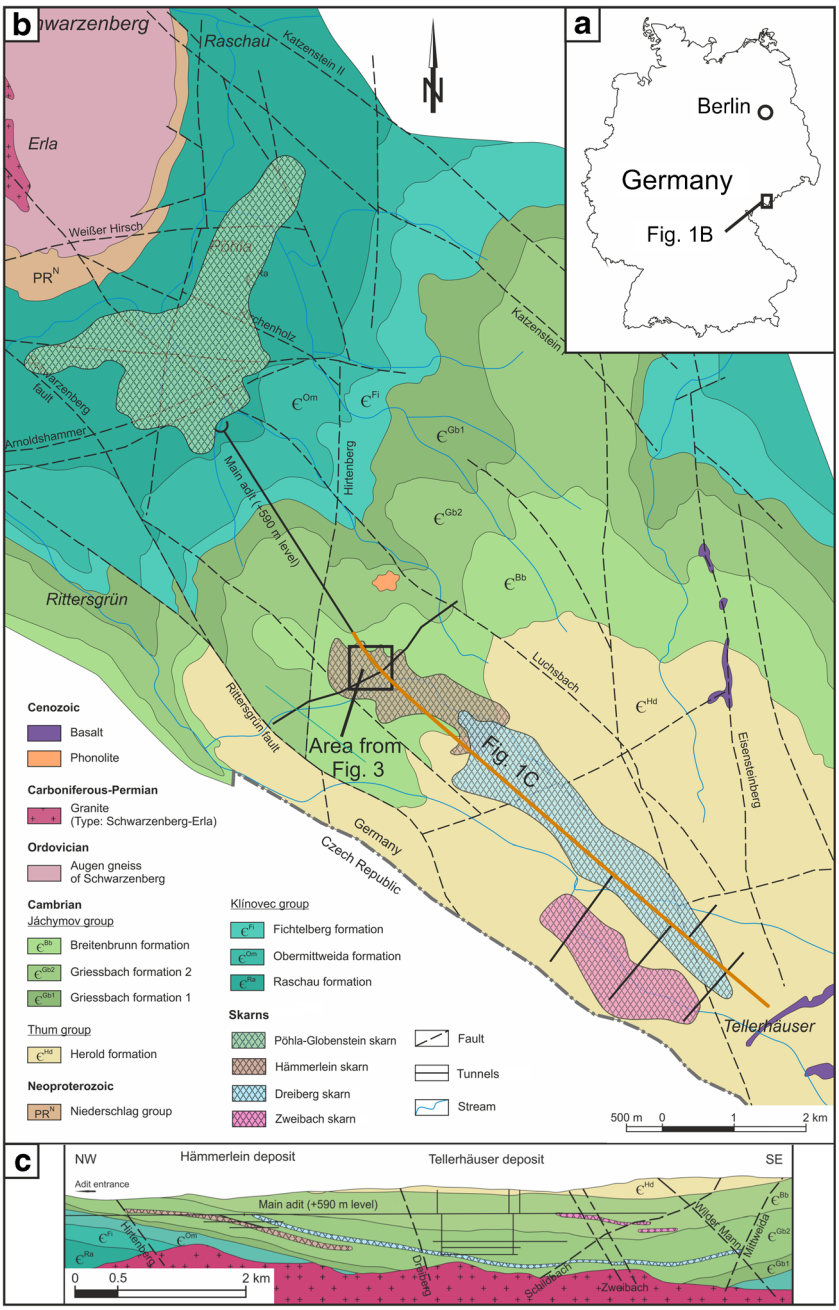

Fig. 1 **a** Overview map of Germany. **b** Regional geological map showing the location of the Hämmerlein skarn (Hämmerlein deposit), the Pöhla-Globenstein skarn (Pöhla-Globenstein deposit) as well as the Dreiberg skarn and Zweibach skarn which are together forming the Tellerhäuser deposit. **c** Geological NW-SE cross-section. Location as indicated in **b** (orange line). Modified after Schuppan and Hiller (2012) and Kästner (2016)

fragment size), jaw crusher (< 0.5 cm fragment size), and impact mill (approximately 95% passing 400 μm).

As part of an ongoing exploration project Saxore Bergbau GmbH collected bulk samples at each of the above-mentioned five sample locations. Several tons of material was recovered for lab-scale and pilot-plant-scale beneficiation experiments. The material was placed into flexible intermediate bulk containers (*big bags*) carrying ~ 1.5 t each. One big bag per location was transferred to UVR-FIA GmbH (Freiberg, Germany), where the material was crushed to 100% < 630 μm with a jaw crusher, a cone crusher, and a sieve ball mill. The five samples were classified into three size fractions (0–100 μm, 100–250 μm, and 250–630 μm).

Methods

For automated mineralogy studies, 30 μm polished thin sections (from hard rock samples) and grain mounts (from crushed samples) were prepared. Analysis was performed with scanning electron microscopy (SEM)-based image analysis using a FEI Mineral Liberation Analyzer (MLA) and bulk geochemical analysis. Geochemical data are used here to

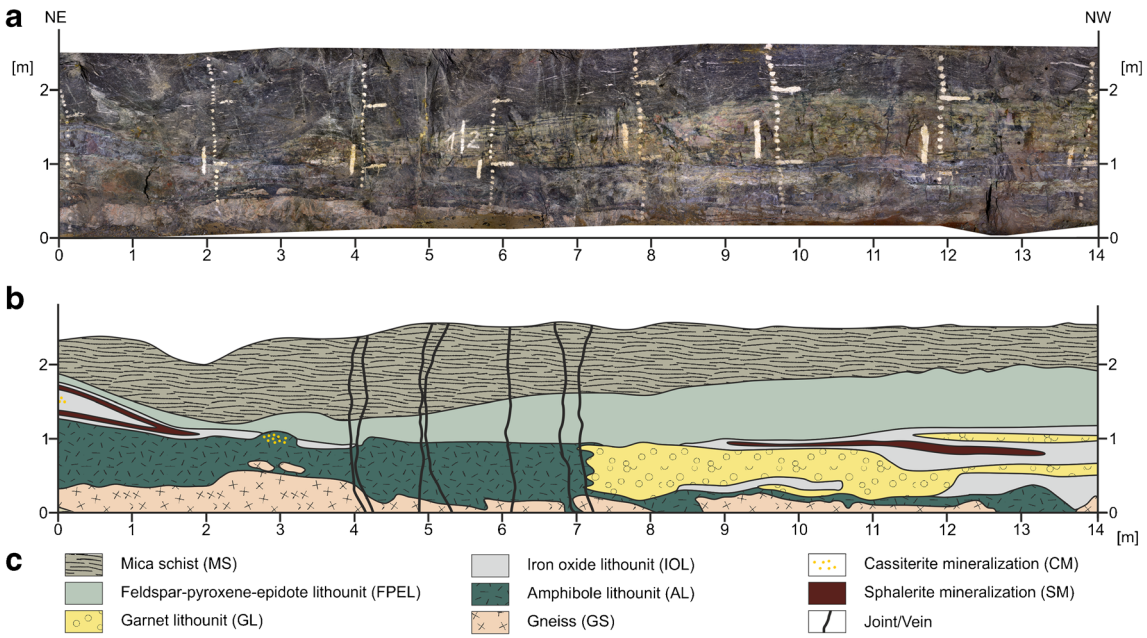

Fig. 2 Underground view of the Hämmerlein deposit. **a** Panoramic photo of the underground situation at Strecke 2-4 (location of the face is indicated in Fig. 3). The white markings are from exploration campaigns during GDR times (between 1970 and 1990). **b** Face map from Strecke 2-4 illustrating geological relations between the different skarn lithounits, mineralization types, and host rocks. **c** Legend. Modified after Kästner (2016)

validate MLA data. The method described by Kern et al. (2018) was applied for MLA analysis, with the only adjustment that the recognition and distinction of chlorite varieties and chemically similar minerals (mica and amphibole) was improved. This was achieved by distinguishing characteristic intensities of iron, magnesium, and potassium peaks in X-ray spectra acquired by energy dispersive spectrometry.

Due to the diversity of the mineral assemblage, it was decided to report modal mineralogy in mineral groups. This was done for simplification and without compromising the

Fig. 3 Underground map of the + 590 m level of the Hämmerlein deposit and the sampled locations; S2-4 = Strecke 2-4, S2-6b = Strecke 2-6b, S4 = Strecke 4, Q2 = Querschlag 2, HS = Hauptstollen. Modified after Kästner (2016)

characteristic attributes of each sample. If further distinction of minerals within a particular group was deemed necessary, this has been noted in the text or figure captions. Of particular importance is the distinction of different members of the chlorite group. Three types of chlorite have been distinguished:

- Chlorite 1 (Fe/Mg 1:2; clinochlore—determined by XRD)
- Chlorite 2 (Fe/Mg 1:1)
- Chlorite 3 (Fe/Mg 2:1; chamosite—determined by XRD)

The Sn deportment is defined as the quantitative distribution of the measured Sn content in a given volume of rock onto different minerals. The lattice-bound Sn that is present in oxide and silicate mineral is summed up and reported as *Sn background* values, as beneficiation to commercially viable mineral concentrates (Pawlek 1983) is not possible for this portion of the contained Sn.

The MAMA ratio

The association of minerals is of particular relevance in this study. Mineral association is a parameter that is readily calculated from MLA data (Gu 2003). The mineral association parameter is defined as the total length of grain boundaries of one mineral A to its associated mineral B—in relation to the total grain boundary length of mineral A (Fig. 4). For particulate samples, the exposed surface (= "free surface") is also taken into consideration. It needs to be stressed here that in this study, free surface is ignored because particulate samples are to be compared to samples that have not been affected by comminution.

Because the mineral association value is highly dependent on the absolute abundance of the associated mineral (mineral B), it is not suited to identify a specific preference of association between mineral pairs. To constrain the preference of association of cassiterite with any of the other minerals (or mineral groups) present, we introduce the following ratio:

$$\mathrm{MAMA}_{\mathrm{target}} = \alpha \frac{\text{Mineral association } (\mathrm{Min}_X) \text{ with target mineral}}{\text{Mineral area } (\mathrm{Min}_X)}$$

with α being a proportionality constant ensuring the average of $\mathrm{MAMA}_{\mathrm{target}}$ for all considered minerals is normalized to 1, making the MAMA ratio a dimensionless quantity. An equivalent ratio was previously also introduced by Smith (2014) without normalizing. For the purpose of this paper, comparing different sample sets, the normalized MAMA ratio is more suitable and easier to acquire.

The MAMA ratio is used to constrain the preference of intergrowth of two minerals. Such preferred association may be either due to a co-genetic origin of two minerals—or indicate a replacive relation. In our case, we only consider the preferred association of cassiterite with gangue minerals. Since cassiterite is not observed to replace pre-existing minerals—and since no younger mineral replaces cassiterite—we can confidently relate high MAMA ratio values to identify co-genetic relationships. Based on the results obtained in this study we consider values for $\mathrm{MAMA}_{\mathrm{cas}} < 0.6$ as preferred disassociation, between 0.6 and 1.4 as ambiguous association and > 1.4 as preferred association.

Results

In the following, textures and mineralogical observations of skarn lithounits and the host rocks are described in context with quantitative mineralogical data acquired by MLA. Observations in the field and under the microscope suggest that the skarn units are metasomatically overprinted by an assemblage of cassiterite-chlorite-fluorite-sulfide; the latter assemblage plays a key role in the genesis of economic Sn mineralization in the Hämmerlein deposit. Further analyses of bulk samples prepared as grain mounts allow calculating the MAMA ratio for cassiterite. This ratio is used to quantify

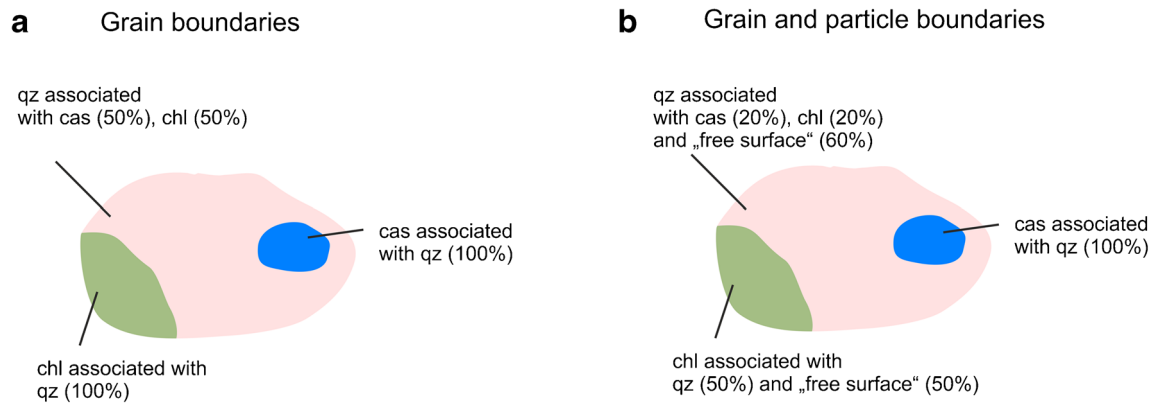

Fig. 4 Mineral associations in a schematic drawing of a particle that consists of quartz (qz), cassiterite (cas) and chlorite (chl). **a** Only grain boundaries between mineral grains are considered. **b** The grain boundaries between the mineral grains and the free surface around the particle are considered

preferred associations between cassiterite and the other minerals from bulk samples.

Characterization of skarn and host rock

Textural and mineralogical characteristics of the skarn lithounits and host rock are described (Figs. 6, 7, and 8) together with modal mineralogy and Sn deportment (Fig. 5a, d). Although the skarn lithounits are named according to their predominant mineral assemblage, it should be stressed that transitions between these units are gradual and irregular (e.g., garnet lithounit and amphibole lithounit).

Observations from hand specimens reveal a heterogeneous distribution of sphalerite and cassiterite within the orebody (Fig. 9). Therefore, bulk samples are used to acquire modal mineralogy, Sn deportment and mineral association data in mineralized rocks (Fig. 5b, c, e; find data in ESM). The samples from locations Q2, S2-6b, and S4 represent skarn with cassiterite mineralization (Skarn w. CM), bulk sample S2-4 represents skarn with sphalerite mineralization (Skarn w. SM), and the bulk sample from the Hauptstollen (HS) is mica schist with cassiterite mineralization (Schiefererz).

Sn-bearing silicates and oxides like titanite, epidote, stokesite, amphibole, and other minerals contribute to the Sn background values (definition see above). Together with Sn in cassiterite, the Sn background values add up to the total Sn content of a sample. Kern et al. (2018) have noted that the total values calculated by MLA compare very well to XRF data with deviations of ± 30% for samples < 0.1 wt% Sn and ± 10% for samples > 0.1 wt% Sn.

Mica schist

The hanging wall and footwall of the skarn succession comprise uniform dark-gray medium- to coarse-grained (0.2–4 mm) and foliated mica schist (MS) of the Breitenbrunn Formation (Fig. 6a) (Schuppan and Hiller 2012). The mica schist is composed of feldspar (38 wt%), mica (30 wt%), quartz (24 wt%), chlorite (4 wt%), and up to 5 mm large euhedral Fe-Al-rich garnet crystals (2 wt%) (Fig. 5a). Sn-bearing minerals are nearly absent (Fig. 5d). Only single

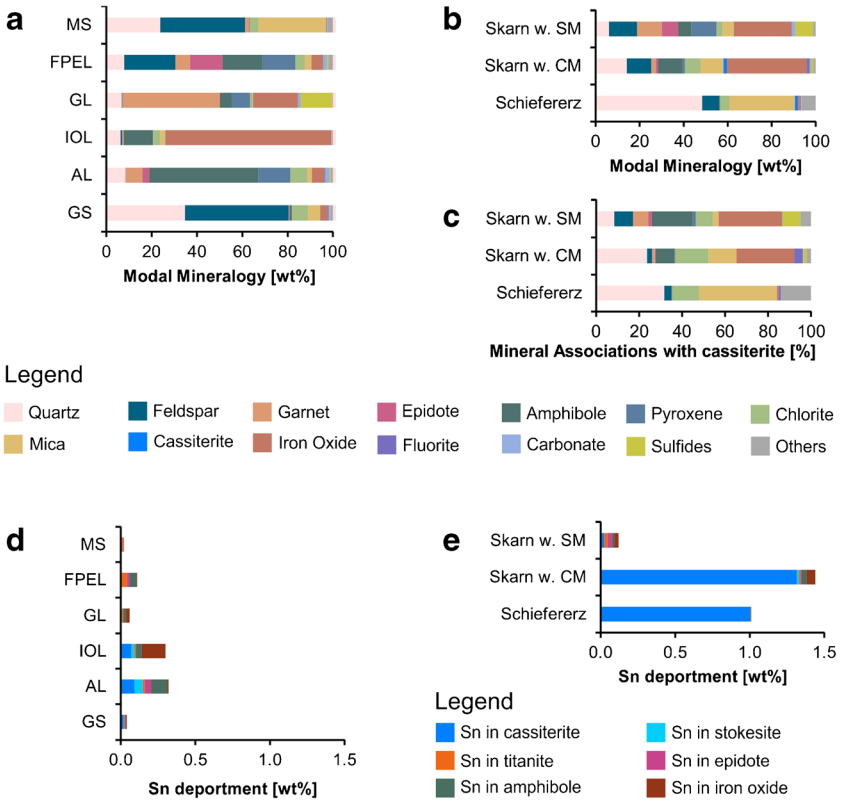

Fig. 5 Modal mineralogy, mineral associations with cassiterite and Sn deportment determined from grain mounts by MLA. **a** Modal mineralogy of lithounits. **b** Modal mineralogy of bulk samples. **c** Mineral associations of bulk samples. **d** Sn deportment of lithounits. **e** Sn deportment of bulk samples. Only samples devoid of the characteristic cassiterite mineralization assemblage (cassiterite-chlorite-fluorite-sulfides) were considered for the calculation of modal mineralogy and Sn deportment of the skarn lithounits (FPEL, GL, IOL, AL). The other mineral in **b** and **c** from the Schiefererz is 99% tourmaline. Abbreviations: MS = mica schist, FPEL = feldspar-pyroxene-epidote lithounit, GL = garnet lithounit, IOL = iron oxide lithounit, AL = amphibole lithounit, GS = gneiss, SM = sphalerite mineralization, CM = cassiterite mineralization. A table with all values can be found in the ESM

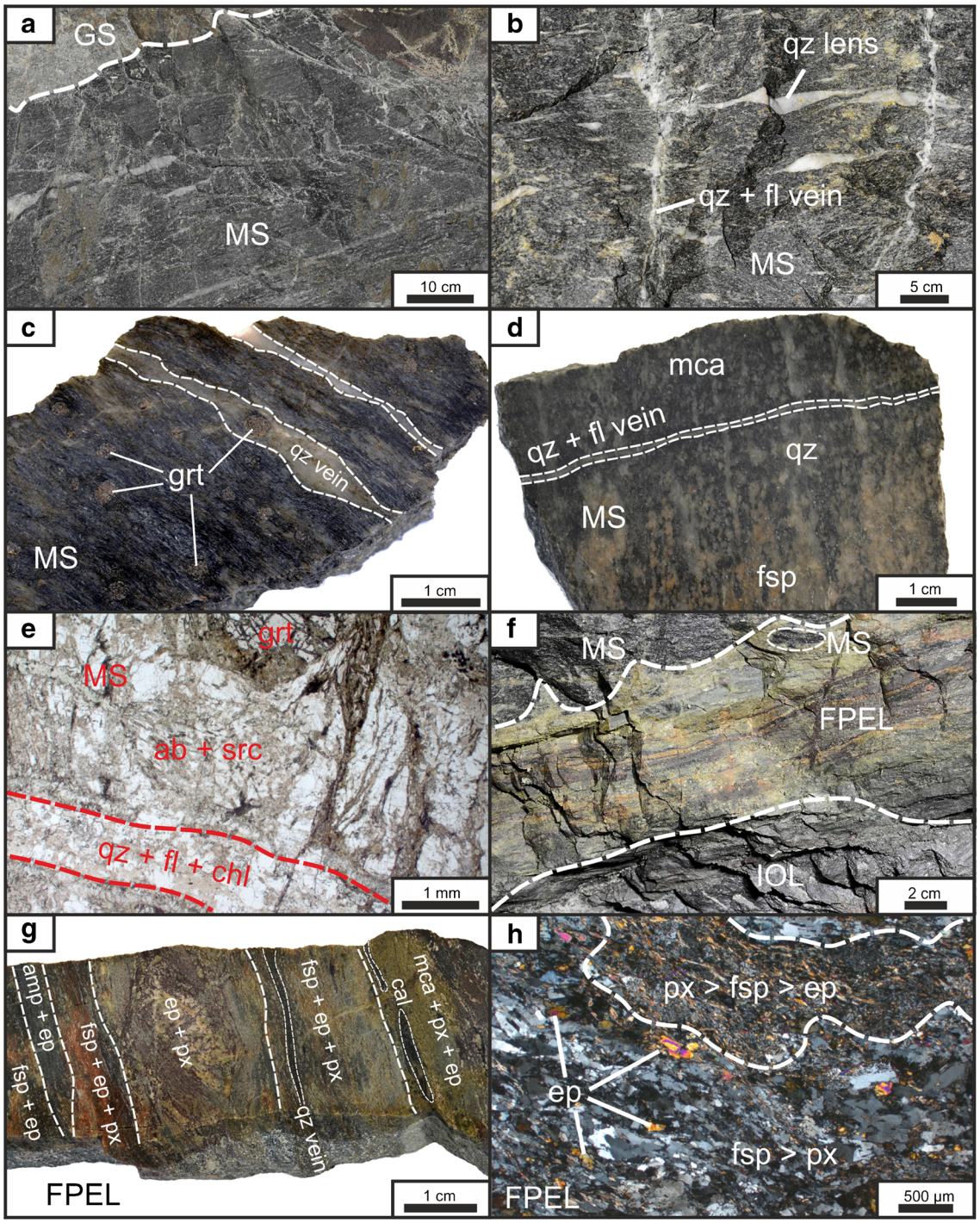

Fig. 6 Unmineralized skarn and host rock I (MS and FPEL). **a** MS with several cm-thick quartz lenses (white-gray) and veins in sharp contact to GS in the hanging wall. **b** MS with horizontal quartz lenses crosscut by sub-vertical quartz veins. Feldspar (yellow) is strongly altered. **c** Polished hand specimen of the MS with foliation and medium- to coarse-grained mica (dark-gray), quartz (milky-gray), feldspar (white), and garnet (red-brown). **d** Polished hand specimen of strongly altered and medium- to coarse-grained MS with a dense foliation with mica (black), quartz (gray), and feldspar (light orange). A 1-mm-thick quartz-fluorite vein crosscuts the foliation in perpendicular direction. **e** Photomicrograph (plane-polarized light) of strongly altered MS with garnet altered to biotite and anorthite (center top) and sercitic albite (center). A late quartz-fluorite-chlorite vein crosscuts the altered MS. **f** FPEL in sharp contact with the IOL. The contact with the MS in the hanging wall is irregular with some MS embedded in the FPEL. **g** Polished hand specimen from the FPEL showing very fine-grained purple-reddish, orange, and light green layers with alternating concentrations of feldspar, pyroxene, epidote, amphibole and mica, and sometimes quartz and calcite. **h** Photomicrograph (cross-polarized light) of the FPEL showing the transition between two layers with alternating amounts of feldspar and pyroxene (50–200 µm) and some epidote (50–500 µm). Abbreviations: MS = mica schist, FPEL = feldspar-pyroxene-epidote lithounit, GS = gneiss, IOL = iron oxide lithounit, qz = quartz, grt = garnet, mca = mica, fl = fluorite, fsp = feldspar, ab = albite, src = sericite, chl = chlorite, ep = epidote, py = pyroxene, cal = calcite

grains of Sn-bearing titanite were identified in one strongly altered sample. Sub-vertical mm- to cm-wide quartz veinlets and few cm-long quartz lenses parallel to the foliation are the most distinct features of the MS (Fig. 6a, c).The contacts to the skarn and gneiss are typically very sharp with a-few-mm-thick transition zones. Varying degrees of alteration have affected the MS which is particularly distinctive within a distance of 60 to 100 cm in the footwall of the skarn. With a higher degree of alteration the feldspars turn to a light orange color (Fig. 6d) and the overall color of the mica schist gets darker (Fig. 6b). Sericitization of albite is observed on microscopic scale (Fig. 6e) as well as alteration from muscovite to biotite and/or chlorite. Furthermore, the alteration is marked by an increased abundance of amphibole, epidote, and calcite. One- to 5-cm-thick veinlets crosscut the altered mica schist; they are orientated perpendicular to the foliation and filled by fluorite and quartz (Fig. 6d), with selvages rimmed by feldspar (mainly anorthite), quartz, chlorite, and some mica.

Mica schist with cassiterite mineralization (Schiefererz)

Schiefererz is mica schist with stockwork-like greisen-style mineralization. One- to 2-cm-thick veinlets filled with an assemblage of quartz, chlorite, fluorite, tourmaline, and relatively coarse-grained cassiterite (of up to 3 mm grain size, Fig. 9g, h). The Schiefererz occurs mostly in the footwall and rarely in the hanging wall of the skarn succession with some of the veinlets reaching directly into the skarn (Fig. 9g). Average Sn content in the Schiefererz is 1.01 wt% (Fig. 5e) which is to 99 wt% derived from cassiterite.

Feldspar-pyroxene-epidote lithounit

The stratabound feldspar-pyroxene-epidote lithounit (FPEL) ranges in thickness between a few cm up to 100 cm. It is fine-grained with a complex mineralogy comprising of feldspar (23 wt%), amphibole (18 wt%), pyroxene (15 wt%), and epidote (14 wt%) accompanied by minor proportions of quartz (8 wt%), garnet (6 wt%), iron oxide minerals (5 wt%), chlorite (4 wt%), mica (3 wt%), and carbonate minerals (2 wt%) (Fig. 5a). This lithounit is typically located in direct contact to the mica schist in the hanging wall and to the garnet or iron oxide lithounit in the footwall (Fig. 6f). Variable amounts of feldspar, pyroxene, epidote, garnet, mica, and amphibole are arranged in sub-horizontal sub-layers with thicknesses from a few mm up to 2 cm. This layering can be observed as a variety of different colors like orange, light- to dark-green, orange-red, gray, and an overall dominant light-olive color which are visible on a macroscopic scale (Fig. 6f, g). The mineral grain sizes range between a few μm and 200 μm but epidote and feldspar grains can be up to 1.5 mm (Fig. 6h). The average whole rock Sn content in hand specimens is 0.11 wt% (Fig. 5d). Titanite, epidote, and amphibole contain significant amounts of Sn, but concentrations are variable and never exceed 3 wt%.

Garnet lithounit

The garnet lithounit (GL) occurs as stratabound lenses of variable size in several locations and lithostratigraphic positions with colors varying from light yellow to yellow-brown. The mineralogy is dominated by garnet (43 wt%), but iron oxide minerals (20 wt%), sulfides (mostly sphalerite, 14 wt%), pyroxene (8 wt%), quartz (7 wt%), and amphibole (5 wt%) also occur (Fig. 5a). The GL is located in the upper half of the skarn succession, often with the feldspar-pyroxene-epidote lithounit in the hanging wall and the iron oxide lithounit in the footwall, but also with the IOL in the hanging wall and the amphibole lithounit in the footwall (Fig. 7a). The thickness of the garnet lithounit lenses averages 40 cm and ranges between 10 and 100 cm. The transition between the garnet lithounit and other lithounits (e.g., IOL and AL, Fig. 7a–c) are irregular gradational. Smaller garnet-dominated lenses or layers occur in other lithounits (Fig. 7a). The garnet in the GL is 70 vol% grossular (Ca-Al-rich) and 30 vol% andradite (Ca-Fe-rich) with grain sizes between 0.1 and 3 mm. The GL averages 0.06 wt% Sn in whole rock samples, which is mostly due to Sn-bearing iron oxide minerals and amphibole (Fig. 5d). The median value for Sn incorporated in the crystal lattice of garnet is ≤ 0.1 wt%.

Iron oxide lithounit

The iron oxide lithounit (IOL) has a very dense and compact appearance with steel-gray color and semi-metallic luster (Fig. 7a). The thickness of the lithounit reaches up to 1.5 m and averages 80 cm. The contact to the feldspar-pyroxene-epidote lithounit in the hanging wall is typically very sharp (Fig. 6 F) but gradational contacts are developed to AL and GL (Figs. 7a and 8a, b). Magnetite and hematite together add up to 73 wt% within the IOL (note that the two minerals are summarized as *iron oxide minerals* in this study). Other significant minerals are amphibole (13 wt%), quartz (6 wt%), chlorite (3 wt%), and mica (2 wt%) (Fig. 5a). Fine-grained anhedral magnetite predominates with isolated subhedral and euhedral grains up to 0.5 cm in size. Along grain boundaries, magnetite is commonly altered to hematite (Fig. 8e, f). The alteration from magnetite to hematite is more distinctive within a radius of a few cm to other lithounits resulting in fine-grained clusters of reddish hematite intergrown with silicate minerals like amphibole, quartz and garnet (Fig. 8b). The average Sn content in whole rock samples is 0.30 wt% (Fig. 5d), which is mostly contained in the crystal lattice of iron oxide minerals, amphibole, and some isolated cassiterite grains (> 5 μm). Cassiterite also appears as

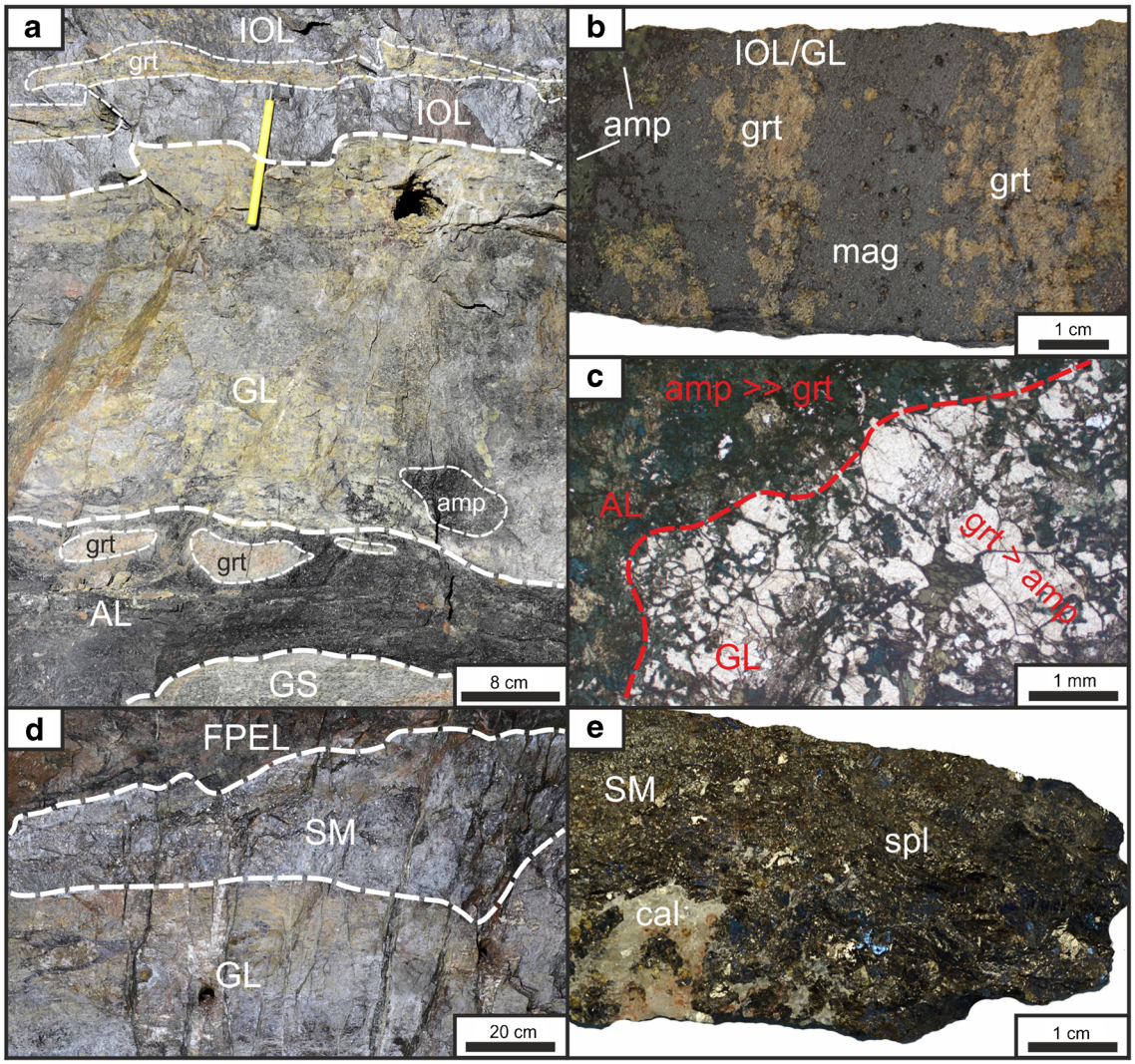

Fig. 7 Unmineralized skarn and host rock II (GL and SM). **a** Several stratabound skarn layers (from top to bottom IOL, GL, AL) with irregular contacts and transition zones and GS in the hanging wall. The GL has a light yellow to gray color. Three lenses of garnet (grt) in the AL have pale yellow to orange color. An amphibole lens (amp) is found in the GL as well as a garnet band (grt) in the IOL. **b** Polished hand specimen from the transition zone between the IOL and GL composed of magnetite and garnet with small amounts of amphibole (amp). **c** Photomicrograph (plane-polarized light) from the contact between the GL and AL. Small amounts of amphibole are present in the GL and garnet is present in the AL. D. Sphalerite mineralization (SM) of 20–40 cm thickness between FPEL and GL. **e** Hand specimen with coarse-grained sphalerite (spl, dark-brown) and white calcite (cal, bottom left). Abbreviations: IOL = iron oxide lithounit, GL = garnet lithounit, AL = amphibole lithounit, FPEL = feldspar-pyroxene-epidote lithounit, SB = sphalerite band, grt = garnet, amp = amphibole, mag = magnetite, cal = calcite, spl = sphalerite

minute (10–200 nm; measured with SEM) inclusions within magnetite and hematite (Fig. 8f).

Amphibole lithounit

The dark-green to black amphibole lithounit (AL) is typically located between the iron oxide lithounit and the gneiss (Fig. 8a). Major minerals are amphibole (48 wt%) and pyroxene (14 wt%) with minor quartz (8 wt%), chlorite (8 wt%), garnet (7 wt%), iron oxide minerals (5 wt%), epidote (3 wt%), carbonate minerals (2 wt%), and mica (2 wt%) (Fig. 5a). The average thickness of the AL is 80 cm, but amphibole accumulations also appear as a-few-cm-thick lenses within the IOL or GL (Fig. 7a). The contact to other lithounits is irregular and alternating with adjacent lithounits. The amphibole lithounit is in a remarkable relation with the gneiss in the footwall (see below), which is intersected by amphibole-chlorite-bearing veins that reach into the amphibole lithounit (Fig. 8a). The abundance of light- to dark-green amphibole and dark-green to black chlorite (chlorite 1 and 2; see the "Methods" section), both with a granular, radial-columnar or flaky habit, are the most distinct attribute of the amphibole lithounit. The

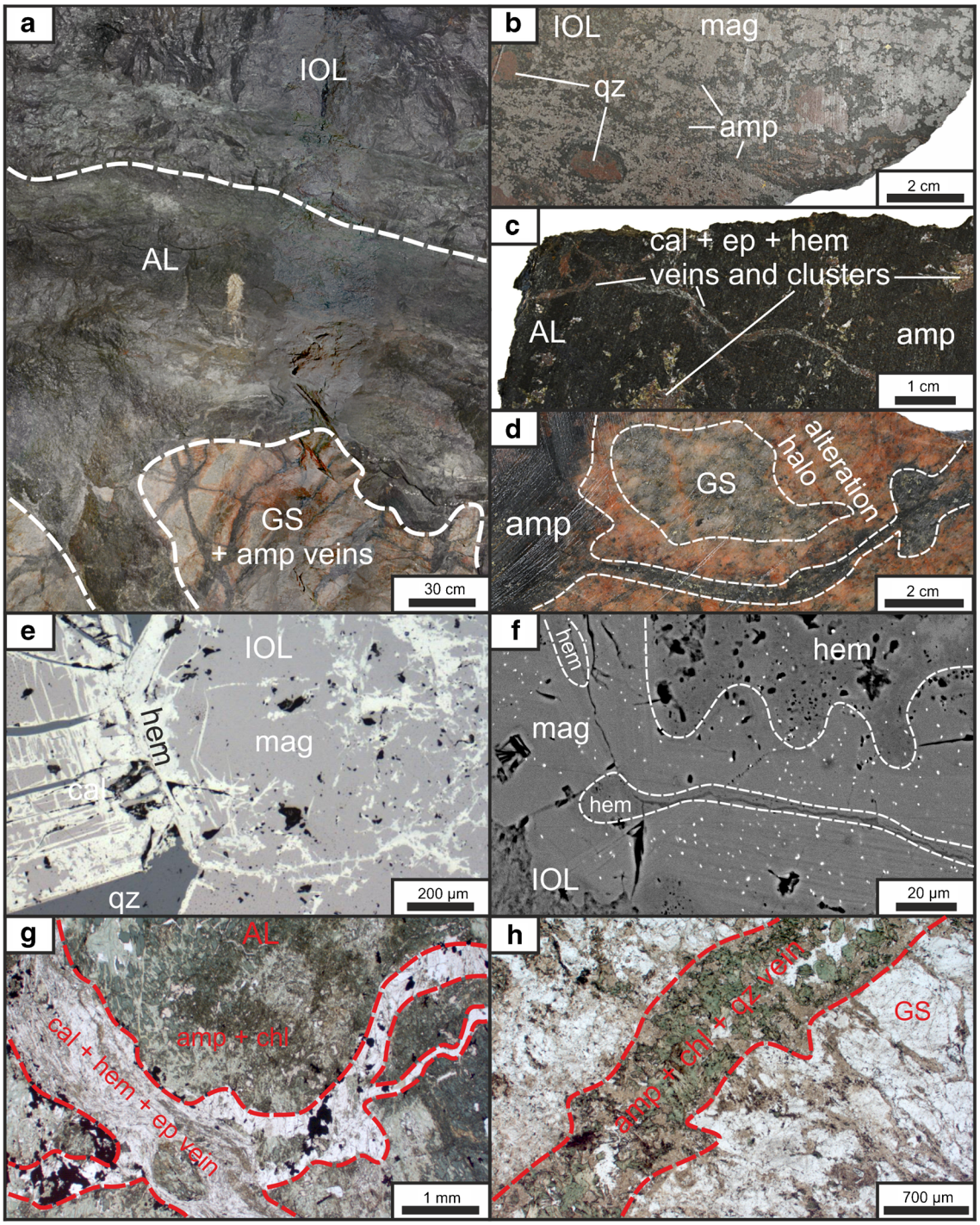

Fig. 8 Unmineralized skarn and host rock III (IOL, AL, and GS). **a** Sharp contact between the IOL and AL. The transition between the AL and GS is irregular. Veins of amphibole crosscut the GS. The white spot in the center is a marking from mine workings. **b** Polished hand specimen from the IOL transitioning to the AL with magnetite (metallic gray), amphibole (dark green) and reddish quartz aggregates (Ø 1–5 cm). **c** Polished hand specimen from the AL composed of mostly amphibole that is partly altered to chlorite (both dark green) and crosscut by veins and clusters of calcite, hematite, epidote, and stokesite. **d** Polished hand specimen of altered gneiss that is crosscut and overprinted by amphibole veins. An alteration halo with iron staining between the GS and the striking amphibole vein has developed. **e** 0.5–3 mm large steel-gray euhedral magnetite grains with martitized rims (=hematite) from the IOL. **f** Back-scattered electron image of the IOL with zonation patterns of magnetite and martitization along cracks. Minute cassiterite grains (bright spots; 10–100 nm) occur preferably in magnetite but occasionally also in hematite. **g** Photomicrograph (plane-polarized light) of a calcite-hematite-epidote vein crosscutting the AL. Amphibole is partially altered to chlorite. **h** Photomicrograph (plane-polarized light) of an amphibole-chlorite-quartz vein crosscutting altered gneiss. Abbreviations: IOL = iron oxide lithounit, AL = amphibole lithounit, GS = gneiss, amp = amphibole, qz = quartz, mag = magnetite, hem = hematite, cal = calcite, ep = epidote

amphibole is commonly altered to chlorite (Fig. 8c, g). During this process, Sn contained in the amphibole is reprecipitated in iron oxide minerals, epidote and stokesite in calcite veins. The total Sn content of 0.32 wt% is thus not only related mostly to Sn-bearing amphibole but also cassiterite and small amounts of Sn-bearing titanite, epidote, and stokesite (Fig. 5d).

Gneiss

Gneiss (GS) comprises the footwall of the skarn succession. It is composed of feldspar (54 wt%, albite and orthoclase), quartz (36 wt%), and mica (9 wt%, mostly muscovite) (Fig. 5a). It is monotonous light-gray-colored and foliated granitic gneiss with medium to coarse grain sizes and up to 5 mm-long feldspar and quartz grains. The thickness ranges from 30 cm up to 1.5 m, averaging 1 m. Contacts to the MS and IOL are mostly sharp. Within a distance of 0–150 cm below the contact to the amphibole lithounit, the gneiss is crosscut by a stockwork of amphibole-rich veins (0.5–5 cm) that reach into the AL. The veins are surrounded by a distinct alteration halo of hematite staining (Fig. 8d). Sn-bearing minerals are absent in the gneiss itself. The Sn content shown in the modal mineralogy is derived from the amphibole-rich veins which contain minor amounts of Sn-bearing minerals (Fig. 5d).

Skarn with cassiterite mineralization (skarn w. CM)

Cassiterite mineralization occurs in veinlets (Fig. 9b) with thicknesses of 1 mm to 5 cm or, more rarely, as irregular-shaped pods and lenses with a maximum diameter of 10–20 cm (Fig. 9a, d). Although this style of cassiterite mineralization is observed in every skarn lithounit described above, it is most common in the iron oxide lithounit and amphibole lithounit (e.g., Fig. 9f). Cassiterite grains range between 5 μm and 3 mm (Fig. 9d) and often show internal zonation patterns under the optical microscope. Cassiterite-bearing veinlets are marked by an assemblage of abundant chlorite 3 (Fe/Mg 2:1), fluorite, chalcopyrite, arsenopyrite, and pyrite. This assemblage is locally accompanied by quartz, iron oxide minerals (magnetite and/or hematite), and carbonate minerals (calcite and/or ankerite). Chlorite is usually very dark-gray/green in color (Fig. 9b, c) but may locally also have a prominent light green color (Fig. 9a). It has an earthy luster and the crystals form a granular to flaky habit. Fluorite is colorless or violet and has grain sizes of up to 1 mm. The abundance of sulfide minerals may be used to recognize the occurrence of much less conspicuous cassiterite during face mapping.

Skarn with sphalerite mineralization (skarn w. SM)

Coarse-grained and dark-brown sphalerite occurs in the garnet lithounit and the iron oxide lithounit. It is commonly intergrown with magnetite and garnet (Fig. 7d) and sometimes associated with quartz and calcite (Fig. 7e). Locally, the sphalerite occurs as a stratabound band parallel to the skarn succession with a thickness ranging from a few cm up to 40 cm; this band may be laterally continuous for 10's of meters. Importantly, the coarse-grained sphalerite is not associated with the other sulfide minerals (chalcopyrite, arsenopyrite, or pyrite) (Fig. 5c).

MAMA ratio for cassiterite

The MAMA ratio as defined above is applied to provide a quantitative measure for the association of cassiterite ($MAMA_{cas}$). Although the ratio could also be applied to any of the other minerals, it is cassiterite that is the primary ore mineral in the Hämmerlein deposit. $MAMA_{cas}$ is calculated for every mineral in all five bulk samples (Table 1). The geometric mean is calculated for the samples Q2, S2-6b, and S4 because they belong to the same ore type (= skarn with cassiterite mineralization). Sample S2-4 (= skarn with sphalerite mineralization) is examined individually because it represents skarn with very low and uneconomic Sn concentrations (Cas = 0.03 wt%). The third ore type is the Schiefererz, which is in direct contact to the skarn ore. $MAMA_{cas}$ for the different ore types is illustrated in Fig. 10. Minerals are sorted for lowest to highest geometric mean values from the samples representing the skarn with cassiterite mineralization.

Results highlight much greater values for chlorite (2.25), fluorite (2.03), and sulfide minerals (2.09)—as compared to other gangue minerals. This agrees with petrographic observations as well as MLA data obtained for the suite of hand specimens (Figs. 6, 7, 8, and 9). The preferred association of cassiterite with fluorite, chlorite, and sulfides (other than sphalerite) is evident for all scales of sampling and for grain mounts as well as polished thin sections prepared from hand specimens. Epidote, garnet, pyroxene, mica, and feldspar are marked by low $MAMA_{cas}$ values, whereas moderate values are recorded for iron oxide minerals, amphibole, quartz, and calcite.

The Schiefererz (1.00 wt% Sn in cassiterite) as well as the sphalerite-mineralized skarn (0.02 wt% Sn in cassiterite) show very similar trends with high $MAMA_{cas}$ for chlorite and fluorite and low $MAMA_{cas}$ for typical prograde skarn minerals. Most values are within the min-max range of the skarn samples with cassiterite mineralization. In the Schiefererz, epidote and iron oxide minerals show high preferred associations with cassiterite and ambiguous associations with sulfide minerals. The sample from S2-4 shows elevated values for amphibole but also no preferred association for sulfide minerals.

Discussion

The relationship between cassiterite and the gangue minerals is crucial for the development of a successful mineral processing

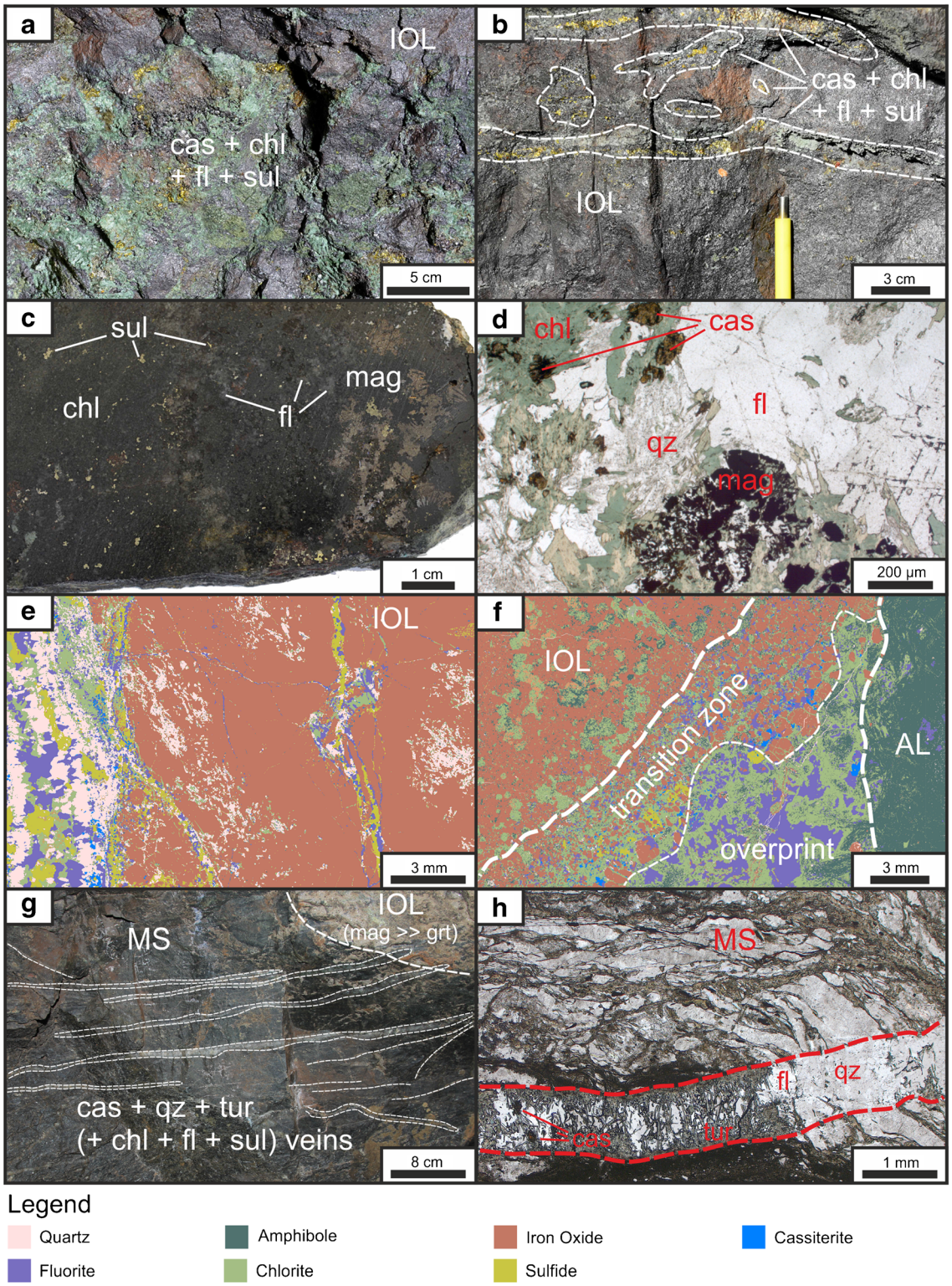

Fig. 9 Cassiterite mineralization in skarn and mica schist. **a** IOL overprinted by assemblage of cassiterte, chlorite (very light green) fluorite (colorless), and the sulfide minerals chalcopyrite, arsenoyprite, and pyrite (yellow-gold; with metallic luster). **b** The same assemblage overprints the IOL forming pods and lenses. **c** Polished hand specimen with chlorite (dark green) fluorite (colorless) and sulfide minerals (metallic/yellow-gold). Cassiterite (< 50 µm) is present but too small to be visible. **d** Photomicrograph (plane-polarized light) with the cassiterite overprint assemblage and additional quartz and magnetite. **e** False-color image by MLA showing veins from the cassiterite overprint crosscutting the IOL. **f** False-color image by MLA showing the cassiterite overprint reaching into the AL and IOL. A transition zone towards IOL has developed. Here, cassiterite is frequently associated with iron oxide minerals even though the phases are not coeval. **g** Numerous quartz- and cassiterite-bearing veinlets crosscut the MS and reach into the skarn (IOL with mag > grt). **h** Tourmaline-fluorite-quartz-cassiterite vein crosscuts the MS. Abbreviations: IOL = iron oxide lithounit, MS = mica schist, cas = cassiterite, chl = chlorite, fl = fluorite, sul = sulfide, tur = tourmaline, grt = garnet, qz = quartz

Table 1 MAMA ratio of cassiterite ($MAMA_{cas}$) from bulk samples; $MAMA_{target} = \alpha$ [mineral association (Min_X) with target mineral / mineral area (Min_X)]; note the similarities between skarn with cassiterite mineralization, skarn with sphalerite mineralization and Schiefererz. The cassiterite content (wt%) in the samples is shown as a reference

Ore type	Skarn w. CM				Skarn w. SM	Schiefererz
Sample location	Q2	S2-6b	S4	Geomean	S2-4	HS
MAMA ratio for cassiterite						
Quartz	**1.50**	0.67	*0.41*	0.81	0.78	*0.51*
Feldspar	*0.26*	*0.22*	*0.04*	*0.14*	*0.34*	*0.34*
Garnet	*0.38*	0.86	*0.24*	*0.47*	*0.51*	*0.24*
Epidote	*0.35*	*0.17*	*0.10*	*0.20*	*0.14*	0.85
Amphibole	0.62	0.96	0.64	0.79	**1.92**	0.63
Pyroxene	*0.54*	*0.54*	*0.23*	*0.44*	*0.08*	NA
Chlorite	**2.52**	**2.17**	**1.60**	**2.25**	**1.74**	**2.73**
Mica	0.89	*0.39*	*0.22*	*0.46*	*0.29*	1.00
Iron Oxide	0.91	1.39	**1.57**	1.37	1.07	**1.73**
Fluorite	**1.86**	**1.42**	**2.43**	**2.03**	**3.11**	**1.53**
Calcite	1.07	**1.69**	*0.37*	0.95	NA	0.60
Sulfides	1.11	**1.52**	**4.15**	**2.09**	1.01	0.85
Average	1.00	1.00	1.00	1.00	1.00	1.00
Cassiterite (wt%)	3.90	0.42	0.41	0.88	0.03	1.27

Low values (≤ 0.6) are shown in italics, high values (≥ 1.4) are in bold

CM cassiterite mineralization, *SM* sphalerite mineralization, *NA* not available, *Geomean* geometric mean

strategy (Petruk 2000). Quantitative data concerning mineralogy, mineral association and microfabric gathered in this study provide evidence for the intimate association of cassiterite with chlorite, fluorite, and certain sulfide minerals. This yields essential clues for beneficiation strategies and also allows drawing important conclusions concerning the genesis of tin mineralization at the Hämmerlein deposit.

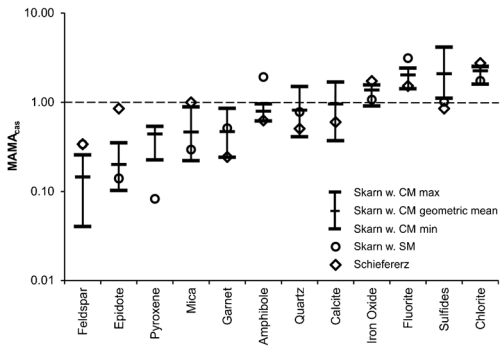

Fig. 10 Minima, maxima, and the geometric mean of $MAMA_{cas}$ for Skarn samples with cassiterite mineralization (Skarn with CM; locations Q2, S4, S2-6b), skarn samples with sphalerite mineralization (Skarn with SM; location S2-4), and mica schist with cassiterite mineralization (Schiefererz, location HS). The dashed line at 1.00 marks the average MAMA ratio of all samples. Minerals are sorted from lowest (left) to highest (right) geometric mean values from the samples representing the skarn with cassiterite mineralization. High geometric mean values (> 1.4) indicate a genetic relationship to cassiterite; a low geometric mean MAMA ratio (< 0.6) indicates the opposite. Values between 0.6 and 1.4 are ambiguous

Tin ore formation

According to Schuppan and Hiller (2012), the geological history of the Hämmerlein deposit and adjacent rocks can be roughly divided into three major stages.

1. Regional metamorphism (amphibolite facies) of sedimentary host rock led to the formation of mica schist, dated to 340 Ma (Kröner and Willner 1998).
2. Skarn formation as a result of the intrusion of an Eibenstock-type granite that led to contact metamorphic alteration, metasomatic overprinting, and the formation of several other skarn and greisen deposits in the area around 320 Ma (Romer et al. 2006; Zhang et al. 2017).
3. Post-Variscan quartz-fluorite-uranium vein mineralization (undated).

The results from this study, particularly the description of the lithounits, the recognition of the cassiterite-bearing assemblage and the preferred association of cassiterite with chlorite, fluorite, and certain sulfide minerals, as quantified and expressed by the MAMA ratio, allow a subdivision of stage 2 (the formation of the skarn) into a prograde and retrograde phase, followed by metasomatic overprint. Similar stages of skarn formation are recognized in many other skarn systems (Meinert et al. 2005).

The FPEL and GL lithounits both have mineral assemblages typical for the 500 to > 700 °C prograde skarn formation (Meinert et al. 2005). These temperatures are favorable for the

formation of minerals with lattice-bound tin (Eadington and Kinealy 1983) rather than cassiterite. Indeed, these two lithounits have low Sn contents (around 0.1 wt%) in bulk samples. The small amount of Sn present is contained in Sn-bearing titanite and epidote. The IOL and AL lithounits as well as the sphalerite mineralization are regarded as a product of a retrograde skarn stage as defined by, e.g., Meinert et al. (2005). These lithounits overprint and replace the prograde skarn lithounits FPEL and GL. An abundance of iron oxide minerals (mostly magnetite) and amphibole with lattice-bound Sn marks this stage.

Alteration of amphibole to chlorites 1 and 2 marks a second stage of retrograde skarn formation. This chloritization is also associated with the formation of Sn-bearing epidote, iron oxide minerals as well as stokesite. This first chloritization event is postdated by another stage of retrograde skarn formation, as expressed by the cassiterite-chlorite-fluorite-sulfide assemblage. Veinlets and lenses with this mineral assemblage crosscut not only pre-existing lithounits of the skarn—a feature described from Sn skarn deposits worldwide (Dobson 1982; Chen et al. 1992; Layne and Spooner 1991)—but also the mica schist (forming Schiefererz). Despite a high variability in modal mineralogy and cassiterite content, $MAMA_{cas}$ shows consistent values in the cassiterite-mineralized skarn, the Schiefererz, and the sphalerite-mineralized skarn. This indicates that cassiterite formation is exclusively related to this one late retrograde event. The concept of two distinct tin mineralization phases (Lefebvre et al. 2018) cannot be confirmed.

Implications for beneficiation

The mineral association parameter as reported by commercially available SEM-based image analysis instruments (Fig. 5c) does not emphasize any preferred association of a (scarce) ore mineral—such as cassiterite—to a (genetically-linked) gangue mineral. Instead, the association parameter is dominated by the influence of the absolute abundance of the gangue mineral in question (see Fig. 9f and the explanation in the figure caption). The MAMA ratio, as introduced in this contribution, quantifies the preferred association between ore and gangue minerals—irrespective of the absolute abundance of the gangue minerals in question. In the case of the Hämmerlein deposit, a significant and consistent preferred association between cassiterite and chlorite, fluorite, and certain sulfide minerals is observed—in excellent agreement with qualitative observations and irrespective of the nature of the sample considered.

Our results illustrate the consistently preferred association between chlorite—as an abundant rock-forming gangue mineral—and cassiterite—an ore mineral of scarce abundance. The abundance of chlorite can thus be used as a robust proxy to estimate the cassiterite content. The assumption is that high abundance of chlorite will correspond to high abundance of associated cassiterite. Likewise, chlorite-poor samples should contain little cassiterite only. A commercially available ore sorter equipped with a short wave infrared (SWIR) detector may then be used to identify and concentrate ore fragments that exceed a pre-defined threshold concentration of chlorite and separate chlorite/cassiterite-rich particles from chlorite/cassiterite-poor particles. Examples of successful discrimination of ore and waste with SWIR and the application of sensor-based sorting using hyperspectral cameras in the mining industry are given in Dalm et al. (2014) and Nienhaus et al. (2014).

The above hypothesis is tested by using the MLA data obtained on a suite of 24 hand specimens that are part of this study. These hand specimens represent the different lithounits and are represented by 24 polished thin sections (analyzed surface is approximately 2.5 × 4.5 cm). The masses of cassiterite and chlorite from the 24 polished thin sections as obtained from MLA data are shown in Fig. 11. The results clearly illustrate that all of the chlorite-poor samples contain little or no cassiterite, while chlorite-rich samples carry the bulk of all cassiterite. Yet, Fig. 11 also illustrates that two of the 24 samples contain abundant chlorite but no cassiterite. These two samples are rich in chlorites 1 and 2, which are formed as a result of amphibole alteration, but which are not associated with cassiterite. Despite these two outliers, it is clear that an industrial sorter capable of concentrating all samples containing more than 10 wt% chlorite will be able to reduce the mass of material for further beneficiation by as much as 68 wt% while reaching a cassiterite recovery of 97 wt%.

It is important to stress that the successful use of ore sorting according to the chlorite content of a sample will only apply to the skarn ores at Hämmerlein. Although the Schiefererz also yielded the preferred association of cassiterite with chlorite, fluorite, and sulfides, the quantitative mineralogy of this ore

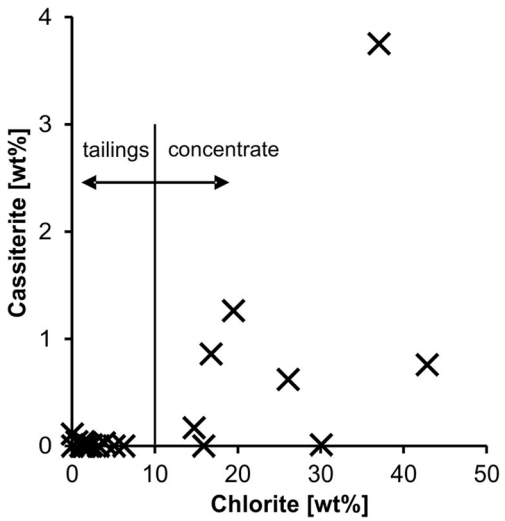

Fig. 11 Cassiterite vs. chlorite content from SEM-based modal mineralogy from 24 thin sections from the Hämmerlein Sn skarn deposit. All specimens that are rich in cassiterite contain chlorite > 10 wt%; separating specimens with > 10 wt% chlorite from specimens with < 10 wt% chlorite could recover 97 wt% of cassiterite in 36 wt% of the whole rock

type is distinctly different, with chlorite present only in very minor quantities—quantities that are too small to be detected by SWIR in an industrial ore sorter. The Schiefererz will thus require a different beneficiation strategy; Schiefererz and skarn ores should thus be considered to be separated by selective mining.

There are other important implications for beneficiation that may be derived from the quantitative mineralogy and microfabric data presented in this study. The intimate association of chlorite and cassiterite, for example, does not only provide an opportunity for ore sorting. In fact, the abundance of chlorite with cassiterite may be expected to be disadvantageous in flotation, because both minerals readily respond to the same reagent regime, thus complicating the separation of the two minerals (Bulatovic 2010). Further difficulties in beneficiation may be related to the abundance of iron oxides, reducing the effectiveness of gravity separation with a falcon concentrator (Buchmann et al. 2017). Another important drawback of the skarn ore is the fine grain size of cassiterite (approximately 50 wt% < 63 μm in bulk samples < 630 μm) in combination with poor liberation of these grains (22 wt% fully liberated). As demonstrated by Astoveza (2017) and (Buchmann et al. 2017), the floatability of cassiterite is limited to a maximum of 50 μm. But any attempt to reach a good degree of liberation of fine-grained cassiterite will also increase the danger of overgrinding. A cautious approach to milling of the skarn ores (Buchmann et al. 2018) may thus have to be combined with innovative separation technologies, such as oil-assisted column flotation (Schach et al. 2017).

Conclusions

The Hämmerlein deposit is an important example of a polymetallic tin skarn deposit that has undergone several stages of ore formation. The fine-grained and mineralogically complex composition of the ores, as well as the variety of lithounits of vastly different composition, render the deciphering of co-genetic mineral assemblages of different ore-forming events difficult by conventional, qualitative approaches. Our study illustrates how quantitative data on mineralogy and microfabric by SEM-based image analysis provides insight into beneficiation characteristics, mineral assemblages and stages of ore formation. The data provides evidence that economically significant tin mineralization—with cassiterite as the ore-forming mineral—at the Hämmerlein deposit is related exclusively to a late metasomatic overprint expressed by the mineral assemblage cassiterite-chlorite-fluorite-sulfides. This characteristic mineral assemblage can be identified in all relevant lithounits that make up the tin resource at the Hämmerlein deposit. The MAMA ratio, defined from SEM-based mineral association and mineral abundance data, reveals the preferred association of (co-genetic) minerals. The same data can also be used to deduce constraints and opportunities for beneficiation. Our case study illustrates the inherent link between ore genesis and process mineralogy—a link that should be considered in any geometallurgical assessment.

Acknowledgements This publication is a contribution to the AFK research project that is funded by the BMBF in the r4 program (grant number: 033R128). Samples for the Hämmerlein deposit were supplied by Saxore Bergbau GmbH. Advice and feedback regarding the samples from Marco Roscher and Lars Starke (both Saxore) is greatly appreciated. Nancy Richter and Martin Miehlbradt are thanked for collecting some of the hand specimens. We would also like to thank Irina Bremerstein from UVR-FIA GmbH for crushing, blending, splitting, and classification of the bulk samples. Furthermore, we would like to thank Gerald van den Boogaart, Markus Buchmann and Edgar Schach for discussions on processing experiments and the MAMA ratio.

References

Astoveza J (2017) Cassiterite flotation and pre-concentration of a fine-grained complex ore. MSc Thesis,Technial University Bergakademie Freiberg

Bauer ME, Seifert T, Burisch M, Krause J, Richter N, Gutzmer J (2017) Indium-bearing sulfides from the Hämmerlein skarn deposit, Erzgebirge, Germany: evidence for late-stage diffusion of indium into sphalerite. Mineral Deposita. https://doi.org/10.1007/s00126-017-0773-1

Bock P (2009) Economic potential of tin, fluorspar and barite occurrences in Saxony. IMRE 3(1):22–31

Buchmann M, Schach E, Bremerstein I, Astoveza J, Kern M, Leißner T, Peuker UA, Rudolph M (2017) Flotation characteristics of a cassiterite bearing complex skarn ore from the Ore Mountains, Germany. Flotation ‘17 Conference, Cape Town, 13–16 November 2017

Buchmann M, Leißner T, Kern M. Schach E, Tolosana-Delgado R, Rudolph M, Gutzmer J, Peuker UA (2018) Fine grinding characteristics of a cassiterite-bearing skarn ore. European Mineral Processing and Recycling Congress (EMPRC), Essen, 25–26 June 2018

Bulatovic SM (2010) Handbook of flotation reagents Vol. II: chemistry, theory and practice: flotation of gold, PGM and oxide minerals. Elsevier, Amsterdam

Chen J, Halls C, Stanley CJ (1992) Tin-bearing skarns of South China—geological setting and mineralogy. Ore Geol Rev 7(3):225–248. https://doi.org/10.1016/0169-1368(92)90006-7

Dalm M, Buxton MWN, van Ruitenbeek FJA, Voncken JHL (2014) Application of near-infrared spectroscopy to sensor based sorting of a porphyry copper ore. Miner Eng 58:7–16. https://doi.org/10.1016/j.mineng.2013.12.016

Dobson DC (1982) Geology and alteration of the Lost River tin-tungsten-fluorine deposit, Alaska. Econ Geol 77:1033–1052. https://doi.org/10.2113/gsecongeo.77.4.1033

Eadington PJ, Kinealy K (1983) Some aspects of the hydrothermal reactions of tin during skarn formation. J Geol Soc Aust 30(3–4):461–471. https://doi.org/10.1080/00167618308729270

Gu Y (2003) Automated scanning electron microscope based mineral liberation analysis. An introduction to JKMRC/FEI Mineral Liberation Analyser. J Miner Mater Charact Eng 2(1):33–41. https://doi.org/10.4236/jmmce.2003.21003

Hösel G (1994) Das Zinnerz-Lagerstättengebiet Ehrenfriedersdorf/Erzgebirge. Bergbau in Sachsen, Band 1, Freiberg

Hösel G (1995) Das Lagerstättengebiet Geyer. Bergbau in Sachsen, Band 4, Freiberg

Hösel G (2003) Die polymetallische Skarnlagerstätte Pöhla-Globenstein. Bergbau in Sachsen, Band 8, Freiberg

ITRI (2016) Report on global tin resources and reserves. Security of long-term tin supply. https://www.itri.co.uk/index.php?option=com_mtree&task=att_download&link_id=55516&cf_id=24 (Accessed 9 July 2018)

Kästner J (2016) Detailed investigations of skarn lithologies and tin mineralisation of the Hämmerlein seam (+590 m level) in the Pöhla-Tellerhäuser ore district (Erzgebirge, Germany). MSc Thesis, Technical University Bergakademie Freiberg

Kern M, Möckel R, Krause J, Teichmann J, Gutzmer J (2018) Calculating the deportment of a fine-grained and compositionally complex Sn skarn with a modified approach for automated mineralogy. Miner Eng 116:213–225. https://doi.org/10.1016/j.mineng.2017.06.006

Kröner A, Willner AP (1998) Time of formation and peak of Variscan HP-TP metamorpishm of quartz-feldspar rocks, Erzgebirge, Saxony. Contrib Mineral Petrol 138:1–20

Layne GD, Spooner ETC (1991) The JC tin skarn deposit, southern Yukon Territory: I. Geology, paragenesis, and fluid inclusion microthermometry. Econ Geol 86:29–47. https://doi.org/10.2113/gsecongeo.86.1.29

Lefebvre MG, Romer RL, Glodny J, Kroner U, Roscher M (2018) The Hämmerlein skarn-hosted polymetallic deposit and the Eibenstock granite associated greisen, western Erzgebirge, Germany: two phases of mineralization—two Sn sources. Miner Deposita. https://doi.org/10.1007/s00126-018-0830-4

Meinert L, Dipple GM, Nicolescu S (2005) World skarn deposits. Econ Geol One Hundredth Anniv:299–336. https://doi.org/10.5382/AV100.11

Miehlbradt M (2017) Mapping and mineral-chemical characterization of the tin-bearing mineralization from the "schist ore" type of the Sn-polymetallic deposit Hämmerlein, distric Pöhla, Germany. MSc Thesis, Technical University Bergakademie Freiberg

Nienhaus K, Pretz T, Wotruba H (2014) Sensor technologies: impulses for the raw materials industry. Shaker Verlag, Aachen

Pawlek F (1983) Metallhüttenkunde. de Gruyter, Berlin, New York

Petruk W (2000) Applied mineralogy in the mining industry. Elsevier, Amsterdam

Romer RL, Thomas R, Stein HJ, Rhede D (2006) Dating multiply overprinted Sn-mineralized granites—examples from the Erzgebirge, Germany. Mineral Deposita 42(4):337–359. https://doi.org/10.1007/s00126-006-0114-2

Schach E, Buchmann M, Leistner T, Kern M, Rudolph M, Peuker UA (2017) Oil assisted column flotation of a cassiterite bearing complex skarn ore from the Ore Mountains, Germany. International Minerals Processing Conference (IMPC), Moscow, 17–21 September 2018

Schuppan W, Hiller A (2012) Die Komplexlagerstätten Tellerhäuser, Uranbergbau und Zinnerkundung in der Grube Pöhla der SDAG Wismut. Bergbau in Sachsen, Band 17, Freiberg

Smith AJB (2014) The geometallurgical characterization of the Merensky Reef at Bafokeng Rasimone Platinum Mine, South Africa. PhD Thesis, University of Johannesburg

Tichomirowa M, Leonhardt D (2010) New age determinations (Pb/Pb zircon evaporation, Rb/Sr) on the granites from Aue-Schwarzenberg and Eibenstock, Western Erzgebirge, Germany. Z Geol Wiss 38(2–3):99–123

Treliver Minerals Limited (2015) Tellerhäuser Project Resource Statement (Press Release). http://www.anglosaxony.com/assets/file/Press%20Release%20Mar%202015.pdf (Accessed 9 July 2018)

van Marcke de Lummen G (1986) Tin-bearing epidote from skarn in the Land's end Aureole, Cornwall, England. Can Mineral 24(2):411–415

Weinhold G (2002) Die Zinnerz-Lagerstätte Altenberg/Osterzgebirge. Bergbau in Sachsen, Band 9, Freiberg

Winkler C (2017) Petrographische und geochemische Charakterisierung der Nebengesteinsalteration im unmittelbaren Kontakt zum Hämmerlein Skarn. BSc Thesis, Technical University Bergakademie Freiberg

Zhang RQ, Lehmann B, Seltmann R, Sun WD, Li CY (2017) Cassiterite U-Pb geochronology constrains magmatic-hydrothermal evolution in complex evolved granite systems: the classic Erzgebirge tin province (Saxony and Bohemia). Geology 45(12):1095–1098. https://doi.org/10.1130/G39634.1